Aerosol Science and Technology

ISSN: 0278-6826 (Print) 1521-7388 (Online) Journal homepage: www.tandfonline.com/journals/uast20

Simulation of Aggregates with Point-Contacting Monomers in the Cluster–Dilute Regime. Part 2: Comparison of Two- and Three-Dimensional Structural Properties as a Function of Fractal Dimension

Rajan K. Chakrabarty, Mark A. Garro, Bruce A. Garro, Shammah Chancellor, Hans Moosmüller & Christopher M. Herald

To cite this article: Rajan K. Chakrabarty, Mark A. Garro, Bruce A. Garro, Shammah Chancellor, Hans Moosmüller & Christopher M. Herald (2011) Simulation of Aggregates with Point-Contacting Monomers in the Cluster–Dilute Regime. Part 2: Comparison of Two- and Three-Dimensional Structural Properties as a Function of Fractal Dimension, Aerosol Science and Technology, 45:8, 903-908, DOI: 10.1080/02786826.2011.568022

To link to this article: https://doi.org/10.1080/02786826.2011.568022

Aerosol Science and Technology, 45:903–908, 2011

ISSN: 0278-6826 print / 1521-7388 online
DOI: 10.1080/02786826.2011.568022

Simulation of Aggregates with Point-Contacting Monomers in the Cluster–Dilute Regime. Part 2: Comparison of Two- and Three-Dimensional Structural Properties as a Function of Fractal Dimension

Rajan K. Chakrabarty,[1,2] Mark A. Garro,[1,2] Bruce A. Garro,[1,2,3] Shammah Chancellor,[1,2] Hans Moosmüller,[1,2] and Christopher M. Herald[4]

[1]*Division of Atmospheric Sciences, Desert Research Institute, Nevada System of Higher Education, Reno, Nevada, USA*
[2]*Sierra Particle Technologies, Reno, Nevada, USA*
[3]*Department of Applied Physics and Applied Mathematics, Columbia University, New York, New York, USA*
[4]*Department of Mathematics and Statistics, University of Nevada, Reno, Nevada, USA*

In the past two decades, several experimental and simulation studies have proposed simple empirical relations between projected two-dimensional (2-D) and three-dimensional (3-D) structural properties of fractal-like aggregates in the cluster–dilute regime. These empirical relations have found extensive use in inferring the 3-D structural properties of aggregates from their projected (i.e., 2-D) properties—measurable from aggregate electron microscopy images. This study probes the limitations and nongeneralizability of these simple and straightforward empirical relationships and proposes replacing them with new empirical formulas. A straightforward empirical relationship for directly determining the 3-D fractal dimension (D_f) of an aggregate from the knowledge of its 2-D aspect ratio is also identified. These new relationships were derived by comparing the ratios of several 2-D and 3-D structural properties of a statistically significant number of simulated aggregates with point-contacting monomers as a function of their 3-D D_f ranging from 1.0 to 3.0 in increments of 0.1.

Received 26 October 2010; accepted 25 February 2011.

This material is based upon work supported by NASA EPSCoR under Cooperative Agreement No. NNX10AR89A, by NASA ROSES under grant NNX11AB79G, by the National Science Foundation under Cooperative Support Agreement No. EPS-0814372, and by the Desert Research Institute. Mark A. Garro, Bruce A. Garro, and Shammah Chancellor acknowledge the support received from Nevada NASA Space Grant program for carrying out part of this research work as interns at Sierra Particle Technologies. Christopher Herald was partially supported by NSF Grant DMS 0709625.

Address correspondence to Rajan K. Chakrabarty, Desert Research Institute, Nevada System of Higher Education, Reno, NV 89512, USA. E-mail: rajan.chakrabarty@dri.edu.

1. INTRODUCTION

The three-dimensional (3-D) fractal dimension, D_f, is considered to be the key property for defining the complex morphology of fractal-like aggregates made of coagulated spherical primary particles (monomers; Cai et al. 1993; Köylü et al. 1995; Oh and Sorensen 1997; Friedlander 2000). The fundamental governing equation connecting D_f with other morphological parameters of a 3-D aggregate is

$$N = k_0(R_g^{3d}/d_p)^{D_f}, \quad [1]$$

where k_0 is the fractal prefactor, d_p is the average monomer diameter, N is the number of monomers, and R_g^{3d} is the radius of gyration of the aggregate. Laboratory investigations and computer simulation studies indicate that the formation of aggregates in high-temperature combustion systems proceed via a 3-D diffusion-limited cluster aggregation (DLCA) growth mechanism (Jullien et al. 1984; Jullien and Botet 1987; Dhaubhadel et al. 2006), and the aggregates asymptotically reach a $D_f \approx 1.8$ (Sorensen 2001; Sorensen and Hageman 2001; Dhaubhadel et al. 2006). While this observation holds true from a theoretical standpoint, in the real world one finds the occurrence of aggregates with D_f significantly deviating from the 1.8 value. Freshly emitted combustion-generated aggregates, which are hygroscopic in nature, undergo morphological restructuring when exposed to high relative humidity in the atmosphere (Zhang et al. 2008; Lewis et al. 2009). These aggregates assume sphere-like morphology, thereby yielding a much higher D_f (close to 3). Recently, an observation was also reported of "stringy" aggregates with lower mass fractal dimension (i.e., D_f

$\approx$ 1.2–1.5) being produced from a premixed flame (Chakrabarty et al. 2009b).

Given the varied morphology that aggregates can assume, experimental techniques to characterize their morphology is of prime interest to researchers. *Ex situ* techniques involving transmission/scanning electron microscopy (TEM/SEM) coupled with digital image analysis have found wide use in determining D_f of aggregates from their projected images (Sorensen 2001; Chakrabarty et al. 2007). The main drawback associated with 2-D ex situ morphology characterization techniques is the difficulty of obtaining key 3-D information about variables such as N and R_g^{3d} required for accurate retrieval of D_f using Equation (1). While these variables are not deducible from a two-dimensional (2-D) image of an aggregate, empirical relationships between measurable 2-D and 3-D properties of aggregates have been derived from simulation and experimental studies to remedy this situation (Samson et al. 1987; Megaridis and Dobbins 1990; Cai et al. 1993; Puri et al. 1993; Köylü et al. 1995; Sorensen and Feke 1996; Oh and Sorensen 1997; Brasil et al. 1999). Brasil et al. (1999) proposed simple empirical relations relating 3-D and projected (i.e., 2-D) properties of a statistically significant number of simulated cluster–cluster fractal-like aggregates. In their study, they considered aggregates to be oriented in random, nonstability-restricted directions. However, in reality, projected properties of the aggregates are analyzed from electron microscopy images, where the aggregates reach a resting position with more than one contact point with the filter surface on which the aggregates are sampled. Hence, it is worth asking if Brasil et al.'s findings are applicable to the aggregates, nonrandomly oriented on a filter surface.

Drawing upon previous findings, this study compares, as a function of D_f, the structural properties of simulated cluster–dilute aggregates (Dhaubhadel et al. 2006)—aggregates with average aggregate–aggregate separation much larger than the aggregate size—in both two and three dimensions. Unlike in previous investigations, in this study, the 2-D properties of the simulated 3-D aggregates were calculated only from their stably oriented projections. This article is the second part in a two-part series, with the first part (Chakrabarty et al. 2011) reporting on the validity, accuracy, and reliability of the most commonly used analysis techniques for the determination of D_f of both individual and ensemble aggregates in the cluster–dilute regime. This manuscript begins with a section describing the simulation technique used in this study for generating a statistically significant number of 3-D aggregates and obtaining their 2-D projections in all possible stable orientations. The section also discusses the various projected structural properties measured for each aggregate projection. This is followed by the results section, which comprehensively discusses our findings on the comparison analysis of 2-D and 3-D aggregate structural properties as a function of D_f. The article concludes by briefly summing up the findings of this study and pointing to the need for future work.

2. SIMULATION AND ANALYSIS OF AGGREGATES

The simulation technique used for this study makes use of a recently developed simulation package, *FracMAP* (Chakrabarty et al. 2008, 2009a), which generates a 3-D fractal aggregate by the particle–cluster aggregation technique with a sequential algorithm that satisfies Equation (1) intrinsically. Although no direct comparison study has been carried out, past simulation studies have used the particle–cluster aggregation technique (Mackowski 1995; Brasil et al. 1999) under the assumption that it generates the same aggregates as the canonical DLCA technique does. For prespecified values of D_f and k_0, the aggregate generation process is initiated by randomly attaching two monomers to each other, followed by the controlled addition of further monomers to the cluster at specific positions fulfilling the following conditions: (1) the monomers do not intersect, i.e., they make point contact, and (2) the radius of gyration of the new aggregate (calculated based on the known positions of the monomers) satisfies Equation (1) for the fractal dimension and prefactor selected (Chakrabarty et al. 2009a). This process is repeated until a preselected monomer number or radius of gyration is reached. The program then identifies all likely resting orientations of the generated 3-D fractal aggregate by assuming a noisy surface (emulating the nonsmooth surface of a TEM/SEM filter) on which the 3-D aggregate center of mass is made to rest above an area defined by the possible contact points of the aggregate. For all the valid stable orientations identified, a pixilated 2-D projection of the 3-D aggregate (similar to a SEM/TEM image) is generated and analyzed for its projected properties.

Simulation runs for this study involved the generation of 3-D fractal aggregates with D_f ranging from 1.0 to 3.0 in increments of 0.1. Sorensen and Roberts (1997) generated aggregates using DLCA and reported values for prefactor k_0 to range between 1.1 and 1.3. On the basis of their findings, a single value of k_0 (1.19) was chosen and kept fixed for all simulation runs conducted as part of this study. There is no universal agreement regarding the value of k_0, and a wide range of k_0 values (between 1.1 and 8) has been reported so far (Farias et al. 1995; Sorensen and Roberts 1997; Heinson et al. 2010). However, in a very recent simulation study, Heinson et al. (2010) showed that the DLCA mechanism yielded aggregates of a broad range of shapes all with $D_f \approx$ 1.8 independent of their shape, but with a shape-dependent k_0. They recommended that aggregates should be described by the pair of parameters D_f and k_0. It was virtually impossible, within normal resource limits, to explore the full parameter space of k_0 for the current simulation study presented here. Variation in k_0 might affect the results and conclusions obtained in this study and is a subject of future research. The monomer diameter d_p used during all the runs was set at a fixed value. For each D_f, at least one hundred 3-D aggregates were generated with the monomer number chosen randomly between 10 and 500 for each aggregate. For each 3-D aggregate generated, all possible stable orientations (Chakrabarty et al. 2009a) of the aggregate

on a 2-D plane were determined. Projections corresponding to the stable orientations for a 3-D aggregate were obtained as 2-D pixilated images and were analyzed for their projected area A_{agg}, projected radius of gyration R_g^{2d}, maximum projected length $L_{\max}^{2d}$, and maximum projected width $W_{\max}^{2d}$ normal to $L_{\max}^{2d}$. Approximately 2500 pixilated images of aggregates for each D_f (a total of ~50,000 images) were analyzed and their various projected structural properties were compared. The resulting comparison data are plotted as a function of D_f using median values and lower and upper quartile designations rather than conventional means and standard deviations, because for certain methods there was heavy skewing of values and outliers on either side of the mean.

3. RESULTS AND DISCUSSION

3.1. Radius of Gyration R_g

As is seen from Equation (1), the radius of gyration R_g^{3d} of a 3-D aggregate is an important property needed for the calculation of D_f. Extracting information about R_g^{3d} of an aggregate from its 2-D image projections has been a daunting challenge for the past three decades. Some studies have used either the radius of gyration in the 2-D plane, R_g^{2d} for calculating D_f or a simple empirical factor to extract R_g^{3d} from R_g^{2d} measurements (Samson et al. 1987; Köylü et al. 1995; Sorensen and Feke 1996). Here, R_g^{2d} of an aggregate image is calculated after the image is threshed using image processing (Chakrabarty et al. 2007). Threshing is a procedure that converts the image into a two-shaded (black and white) image, where black pixels represent parts of the aggregate and white pixels represent everything else (not part of the aggregate). The R_g^{2d} of a single aggregate is then calculated as

$$R_g^{2d} = D_1^{-1} \sum_{x,y} D_1(x, y)(\vec{r}(x, y) - \vec{r}_{cm})^2. \quad [2]$$

In Equation (2), D_1 is the sum of all individual black pixels (or the projected area of the aggregate) designated uniquely by the ordered pairs (x, y), and $\vec{r}_{cm}$ is the position of the aggregate center of mass found by using the following equation:

$$\vec{r}_{cm} = D_1^{-1} \sum_{x,y} D_1(x,y)\,\vec{r}\,(x,y). \quad [3]$$

Figure 1 shows a plot of the ratio of R_g^{2d} and R_g^{3d} as a function of D_f with median values and lower and upper quartile designations. The plot makes it apparent that (1) for any given D_f, R_g^{3d} of an aggregate is always greater than its corresponding R_g^{2d}, calculated from the aggregate's projections for all possible stable resting orientations, and (2) there are many overlapping values of R_g^{2d}/R_g^{3d} for varying values of D_f, thus making it impossible to come up with a one-to-one relationship between the two variables. It is to be noted here that for $D_f = 1.8$, previous

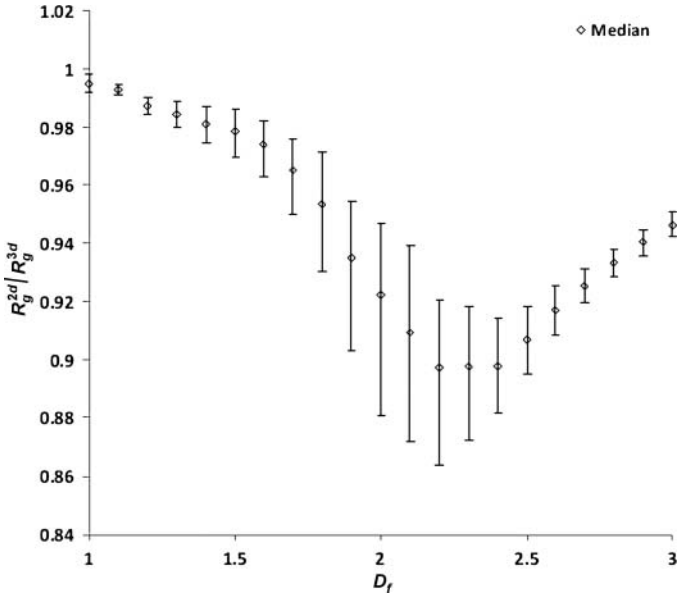

FIG. 1. The ratio of 2-D and 3-D radius of gyration (R_g^{2d}/R_g^{3d}) as a function of 3-D fractal dimension (D_f) with median values and lower and upper quartile designations.

workers have found $R_g^{2d}/R_g^{3d} = 0.91$, which agrees well with our findings (Figure 1) of $R_g^{2d}/R_g^{3d} = 0.93 \pm 0.3$.

Several studies in the past have suggested that R_g^{3d} can be extracted from the projected parameter $L_{\max}^{2d}$, which is easily measured using readily available image processing software (Samson et al. 1987; Puri et al. 1993; Köylü et al. 1995). Puri et al. (1993), using the stereopair agglomerate measurements of Samson et al. (1987), obtained results using a thirty-six-aggregate sample of soot from an acetylene flame and reported $L_{\max}^{2d}/R_g^{3d} = 3.56$. Köylü et al. (1995) experimentally and numerically investigated the projected as well as the 3-D structural properties of soot aggregates and suggested $L_{\max}^{2d}/R_g^{3d} = 2.98$ for aggregates with $N > 100$. Oh and Sorensen (1997) give $L_{\max}^{2d}/R_g^{3d} = 2.90$ for their numerically simulated aggregates. More recently, Brasil et al. (1999), based on their simulation results, suggested $L_{\max}^{2d}/R_g^{3d} = 3.00 \pm 0.10$ for all ranges of N and monomer overlap factors. Figure 2 shows a plot of the ratios of $L_{\max}^{2d}$ and R_g^{3d} as a function of D_f with median values and lower and upper quartile designations. Error bars in this plot are minimal, and the median values of the ratios of $L_{\max}^{2d}$ and R_g^{3d} against D_f is a one-to-one relationship for $D_f < 2$. In the range of D_f between 2 and 3, $L_{\max}^{2d}/R_g^{3d}$ can be treated approximately as a constant of about 2.85 for a range of D_f from 2 to 3.

The values of $L_{\max}^{2d}/R_g^{3d}$ over the whole range of D_f is best described using the second-order polynomial equation:

$$\frac{L_{\max}^{2d}}{R_g^{2d}} = 0.2434^{0.00}_{+0.02}(D_f)^2 - 1.2433^{+0.02}_{-0.09}(D_f) + 4.407^{-0.01}_{+0.06},$$
$$R^2 = 0.99. \quad [4]$$

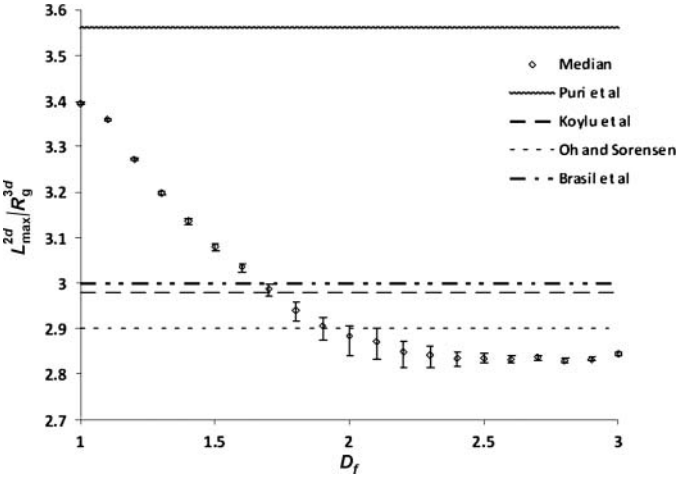

FIG. 2. The ratio of maximum projected length ($L^{2d}_{\max}$) and 3-D radius of gyration (R^{3d}_g) as a function of 3-D fractal dimension (D_f) with median values and lower and upper quartile designations.

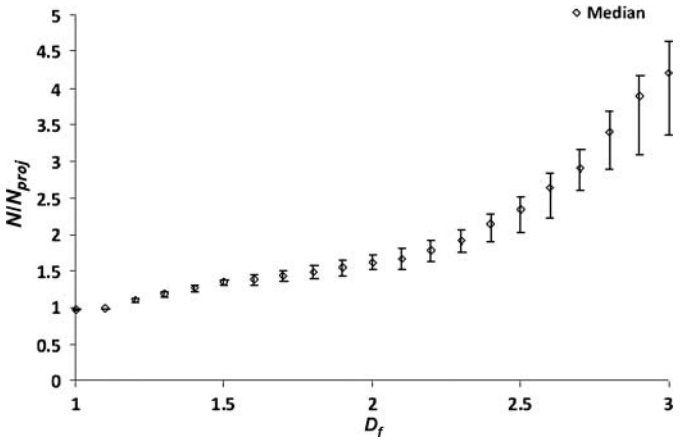

FIG. 3. The ratio of number of monomers in 3-D (N) and projected number of monomers (N_{proj}) as a function of 3-D fractal dimension (D_f) with median values and lower and upper quartile designations.

In Equation (4), the superscripts and the subscripts correspond to the difference between upper and lower quartile values and the mean, respectively. However, the values of $L^{2d}_{\max}/R^{3d}_g$ can be approximated to be 2.98 ± 0.1 in the D_f range between 1.5 and 2, the region where most combustion-generated aggregates are found to exist (Sorensen 2001). For $D_f = 1.8$, the findings from this research agree to within 3% of the findings by previous investigators.

3.2. Number of Monomers (N)

A common practice of determining N of an aggregate for use in Equation (1) is from the 2-D parameter N_{proj}, which is the ratio of the aggregate projected area A_{agg} to the average monomer area A_p (i.e., A_{agg}/A_p). Empirical formulas relating N and N_{proj} have been suggested by several studies in the following format:

$$N \approx (N_{proj})^{\alpha}, \qquad [5]$$

where α is an empirical correction exponent for taking into account the overlap between monomers in aggregates. Also, α is defined for spherical monomers in an aggregate as the ratio of the primary monomer diameter to the distance between the centers of two touching monomers, and its value ranges between 1 and 2. Oh and Sorensen (1997) took into account the varying degrees of monomer overlap and discussed the different values of α that are needed for using Equation (5). Using stereopair observation, Samson et al. (1987) directly determined N for a collection of thirty-nine aggregates for $5 < N < 162$ that were captured from the plume of a smoking diffusion acetylene flame. The values of N_{proj} for the same population were determined with $\alpha = 1.09$ (Megaridis and Dobbins 1990), in agreement with Sorensen et al. who determined $\alpha = 1.09$ for soot from a premixed flame (Cai et al. 1993). Recently, results proposed by Köylü et al. (1995) for soot fractal aggregates based on both numerical and experimental data used the power law of Equation (5), and their least-squares fit value for α was 1.10.

While all the aforementioned studies have suggested a simple exponential correction factor ($\alpha \approx 1.09$) for calculating N from N_{proj}, this study investigated how the ratio of N and N_{proj} varies as a function of D_f for aggregates with point-contacting monomers. Figure 3 shows a plot of the ratio of N and N_{proj} as a function of D_f with median values and lower and upper quartile designations. From the figure, it is obvious that N/N_{proj} is sensitive to variations in D_f, implying that Equation (5) is not applicable over the entire range of D_f. There exists a one-to-one relationship between the two parameters with minimal error bars, especially in the $D_f < 2$ region. The relationship between the two parameters can be best described using the following exponential relationship:

$$\frac{N}{N_{proj}} = 0.46^{-0.01}_{+0.05}(e)^{0.68^{+0.04}_{-0.09}(D_f)}, \quad R^2 = 0.95, \qquad [6]$$

where the superscripts and the subscripts correspond to the difference between upper and lower quartile values and the mean, respectively. Here, while we have only shown that N/N_{proj} is a function of D_f for point-contacting monomers, we also expect a functional D_f dependency for overlapping monomers.

3.3. Aspect Ratio

Aspect ratio is the ratio between the maximum projected width $W^{2d}_{\max}$ and the maximum projected length $L^{2d}_{\max}$ of an object and is one of the most widely used "conventional shape descriptors." Because the aggregate size can be defined in many different ways, a correspondingly large number of conventional shape descriptors exist. Each conventional shape descriptor combines two measures of the aggregate size as a ratio (Hentschel and Page 2003) and is most sensitive to a specific attribute of shape,

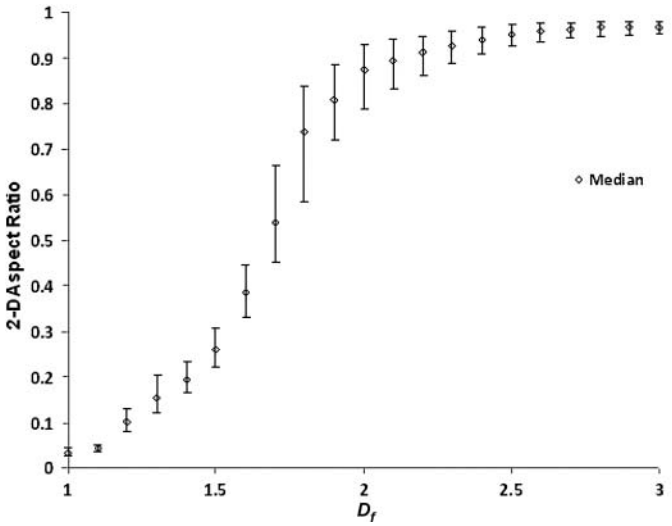

FIG. 4. The 2-D aspect ratio of an aggregate as a function of 3-D fractal dimension (D_f) with median values and lower and upper quartile designations.

depending upon the size measures selected. Aspect ratio is most sensitive to the elongation of an aggregate (Chakrabarty et al. 2006). Figure 4 shows a plot of aggregate aspect ratio as a function of D_f. with median values and lower and upper quartile designations. This plot shows a one-to-one relationship between the two variables with very little ambiguity of inference, especially for the values of D_f between 1 and 2. The empirical formula connecting the two variables is provided below as a piecewise function of linear and power-law functions.

$$\frac{W^{2d}_{\max}}{L^{2d}_{\max}} = 0.47^{+0.08}_{-0.07}(D_f) - 0.46^{-0.07}_{+0.07}, \quad D_f \le 1.15; \quad R^2 = 0.98, \tag{7}$$

$$\frac{W^{2d}_{\max}}{L^{2d}_{\max}} = -1.11^{-0.93}_{+0.82}(D_f)^2 + 5.1751^{+3.28}_{+3.00}(D_f) - 5.028^{-2.78}_{+2.61}, \quad 1.5 < D_f \le 2.0; \quad R^2 = 0.99, \tag{8}$$

$$\frac{W^{2d}_{\max}}{L^{2d}_{\max}} = 0.75^{+0.11}_{-0.14}(D_f)^{0.25^{-0.12}_{+0.19}}, \quad D_f > 2.0; \quad R^2 = 0.90. \tag{9}$$

where the superscripts and the subscripts correspond to the difference between upper and lower quartile values and the mean, respectively. It is interesting to note that the aspect ratio approaches 1 as the aggregates become more spherical—characterized by D_f approaching 3—with $W^{2d}_{\max}$ equaling $L^{2d}_{\max}$. As is apparent, these empirical relationships provide a straightforward way to directly determine the D_f of an aggregate with point-contacting monomers from the knowledge of its two basic projected size ratios—the maximum projected width and the maximum projected length.

4. CONCLUSIONS

In this present work, the nongeneralizability of often-used empirical relationships relating 3-D and projected properties of cluster–dilute aggregates has been highlighted. This was accomplished by comparing the ratios of several projected and 3-D morphological properties of simulated 3-D aggregates as a function of D_f ranging from 1.0 to 3.0 in increments of 0.1. The simulation package, *FracMAP* (Chakrabarty et al. 2008, 2009a), was used for generating a statistically significant number of projected images (∼50,000 total or 2500 per D_f) for all stable orientations of computer-generated 3-D aggregates. These images were analyzed to determine several 2-D aggregate morphological parameters. These parameters were compared with 3-D morphological parameters of the aggregates, and important conclusions were drawn as follows:

(1) For any given D_f, the R^{3d}_g value of a 3-D aggregate is always greater than its projected R^{2d}_g values, and many overlapping values of R^{2d}_g / R^{3d}_g exist for varying values of D_f. Thus, it is not advisable to use projected R^{2d}_g values as replacement for the actual R^{3d}_g value of an aggregate in Equation (1) for calculating D_f.
(2) The ratio of the maximum projected length $L^{2d}_{\max}$ to R^{3d}_g of an aggregate cannot be treated as a constant (i.e., ≈3) for the whole range of D_f; instead it can be best described using a second-order polynomial equation.
(3) For point-contacting monomers, the ratios of N and N_{proj}—which is the ratio of the aggregate projected area A_{agg} to the average monomer area A_p (i.e., A_{agg}/A_p)—vary as a function of D_f with a power-law function. This finding suggests a D_f dependency of the ratio between N and N_{proj} for all values of α, implying the nonapplicability of the well-established exponential correction factor of $\alpha = 1.08$.
(4) Using simple empirical formulae, the D_f of an aggregate can be inferred from the aspect ratio of its projected images.

Finally, future research work is needed in the direction of investigating the relationship between 3-D and projected morphological properties of aggregates as a function of aggregate prefactor k_0, α, and monomer diameter d_p. Variations in these parameters are observed in typical experimental samples (Sorensen 2001; Chakrabarty et al. 2007).

REFERENCES

Brasil, A. M., Farias, T. L., and Carvalho, M. G. (1999). A Recipe for Image Characterization of Fractal-Like Aggregates. *J. Aerosol Sci.*, 30:1379–1389.

Cai, J., Lu, N., and Sorensen, C. M. (1993). Comparison of Size and Morphology of Soot Aggregates as Determined by Light-Scattering and Electron-Microscope Analysis. *Langmuir*, 9:2861–2867.

Chakrabarty, R. K., Garro, M. A., Chancellor, C., Herald, C., and Moosmüller, H. (2009a). FracMAP: A Graphical User-Interactive Package for Performing Simulation and Morphological Analysis of Fractal-Like Aerosol Agglomerates. *Comput. Phys. Commun.*, 180:1376–1381.

Chakrabarty, R. K., Garro, M. A., Garro, B. A., Chancellor, S., Moosmuller, H., and Herald, C. M. (2011). Simulation of Aggregates with Point-Contacting Monomers in the Cluster–Dilute Regime. Part 1: Determining the Most

Reliable Technique for Obtaining Three-Dimensional Fractal Dimension from Two-Dimensional Images. *Aerosol Sci. Technol.*, 45:75–80.

Chakrabarty, R. K., Garro, M. A., Herald, C., and Moosmüller, H. (2008). A User-Interactive Package for Performing Simulation and Orientation-Specific Morphology Analysis of Solid Nano-Agglomerates. *United States Patent USPTO Pub. No. 20100057421-Al.*

Chakrabarty, R. K., Moosmüller, H., Arnott, W. P., Garro, M. A., Slowik, J. G., Cross, E. S., Han, J.-H., Davidovits, P., Onasch, T. B., and Worsnop, D. R. (2007). Light Scattering and Absorption by Fractal-Like Carbonaceous Chain Aggregates: Comparison of Theories and Experiment. *Appl. Opt.*, 46:6990–7006.

Chakrabarty, R. K., Moosmuller, H., Arnott, W. P., Garro, M. A., Tian, G. X., Slowik, J. G., Cross, E. S., Han, J. H., Davidovits, P., Onasch, T. B., and Worsnop, D. R. (2009b). Low Fractal Dimension Cluster–Dilute Soot Aggregates from a Premixed Flame. *Phys. Rev. Lett.*, 102:235504(1)–235504(4).

Chakrabarty, R. K., Moosmüller, H., Garro, M. A., Arnott, W. P., Walker, J. W., Susott, R. A., Babbitt, R. E., Wold, C. E., Lincoln, E. N., and Hao, W. M. (2006). Emissions from the Laboratory Combustion of Wildland Fuels: Particle Morphology and Size. *J. Geophys. Res.*, 111: doi: 10.1029/2005JD006659 DO7204, 1–16.

Dhaubhadel, R., Pierce, F., Chakrabarti, A., and Sorensen, C. M. (2006). Hybrid Superaggregate Morphology as a Result of Aggregation in a Cluster-Dense Aerosol. *Phys. Rev. E*, 73:011404(1)–011404(4).

Farias, T. L., Carvalho, M. G., Koylu, U. O., and Faeth, G. M. (1995). Computational Evaluation of Approximate Rayleigh-Debye-Gans/Fractal-Aggregate Theory for the Absorption and Scattering Properties of Soot. *J. Heat Trans.-T. ASME*, 117:152–159.

Friedlander, S. K. (2000). *Smoke, Dust, and Haze: Fundamentals of Aerosol Dynamics*. Oxford University Press, New York.

Heinson, W. R., Sorensen, C. M., and Chakrabarti, A. (2010). Does Shape Anisotropy Control the Fractal Dimension in Diffusion-Limited Cluster–Cluster Aggregation? *Aerosol Sci. Technol.*, 44:I–IV.

Hentschel, M. L., and Page, N. W. (2003). Selection of Descriptors for Particle Shape Characterization. *Particle and Particle Systems Characterization*, 20:25–38.

Jullien, R., and Botet, R. (1987). *Aggregation and Fractal Aggregates*. World Scientific, Singapore.

Jullien, R., Kolb, M., and Botet, R. (1984). Diffusion Limited Aggregation with Directed and Anisotropic Diffusion. *J. Phys.*, 45:395–399.

Köylü, Ü. Ö., Faeth, G. M., Farias, T. L., and Carvalho, M. G. (1995). Fractal and Projected Structure Properties of Soot Aggregates. *Combust. Flame*, 100:621–633.

Lewis, K. A., Arnott, W. P., Moosmuller, H., Chakrabarty, R. K., Carrico, C. M., Kreidenweis, S. M., Day, D. E., Malm, W. C., Laskin, A., Jimenez, J. L., Ulbrich, I. M., Huffman, J. A., Onasch, T. B., Trimborn, A., Liu, L., and Mishchenko, M. I. (2009). Reduction in Biomass Burning Aerosol Light Absorption upon Humidification: Roles of Inorganically-Induced Hygroscopicity, Particle Collapse, and Photoacoustic Heat and Mass Transfer. *Atmos. Phys. Chem.*, 9:8949–8966.

Mackowski, D. W. (1995). Electrostatic Analysis of Radiative Absorption by Sphere Clusters in the Rayleigh Limit: Application to Soot Particles. *Appl. Opt.*, 34:3535–3545.

Megaridis, C. M., and Dobbins, R. A. (1990). Morphological Description of Flame-Generated Materials. *Combust. Sci. Technol.*, 71:95–109.

Oh, C., and Sorensen, C. M. (1997). The Effect of Overlap between Monomers on the Determination of Fractal Cluster Morphology. *J. Colloid Interface Sci.*, 193:17–25.

Puri, R., Richardson, T. F., Santoro, R. J., and Dobbins, R. A. (1993). Aerosol Dynamic Processes of Soot Aggregates in a Laminar Ethene Diffusion Flame. *Combust. Flame*, 92:320–333.

Samson, R. J., Mulholland, G. W., and Gentry, J. W. (1987). Structural Analysis of Soot Agglomerates. *Langmuir*, 3:272–281.

Sorensen, C. M. (2001). Light Scattering by Fractal Aggregates: A Review. *Aerosol Sci. Technol.*, 35:648–687.

Sorensen, C. M., and Feke, G. D. (1996). The Morphology of Macroscopic Soot. *Aerosol Sci. Technol.*, 25:329–337.

Sorensen, C. M., and Hageman, W. B. (2001). Two-Dimensional Soot. *Langmuir*, 17:5431–5434.

Sorensen, C. M., and Roberts, G. C. (1997). The Prefactor of Fractal Aggregates. *J. Colloid Interface Sci.*, 186:447–452.

Zhang, R. Y., Khalizov, A. F., Pagels, J., Zhang, D., Xue, H. X., and McMurry, P. H. (2008). Variability in Morphology, Hygroscopicity, and Optical Properties of Soot Aerosols during Atmospheric Processing. *Proc. Natl. Acad. Sci. U. S. A.*, 105:10291–10296.